

First Constraints on the Complete Neutrino Mixing Matrix with a Sterile Neutrino

G.H. Collin¹, C.A. Argüelles^{1*}, J.M. Conrad¹, and M.H. Shaevitz²

¹ *Massachusetts Institute of Technology, Cambridge, MA 02139, USA and*

² *Columbia University, New York, NY 10027, USA*

Neutrino oscillation models involving one extra mass eigenstate beyond the standard three (3+1) are fit to global short baseline experimental data and the recent IceCube $\nu_\mu + \bar{\nu}_\mu$ disappearance search result. We find a best fit of $\Delta m_{41}^2 = 1.75 \text{ eV}^2$ with $\Delta\chi_{\text{null-min}}^2$ (dof) of 50.61 (4). We find that the combined IceCube and short baseline data constrain θ_{34} to $< 6^\circ$ at 90% CL for $\Delta m_{41}^2 > 2 \text{ eV}^2$, which is a factor of two improvement beyond the present limit. Incorporating the IceCube information provides the first constraints on all entries of the 3+1 mixing matrix.

PACS numbers: 14.60.Pq, 14.60.St

INTRODUCTION

Neutrino oscillations are due to quantum-mechanical effects that occur if the neutrino mass eigenstates are mixtures of the neutrino flavor eigenstates. These effects have been observed in multiple experiments [1]. Most neutrino oscillation data sets fit well into a model involving three active neutrinos that map to three distinct mass states through a unitary mixing matrix [1]. This three-neutrino model, then, has two independent squared-mass splittings, $\Delta m_{ji}^2 = m_j^2 - m_i^2$. The frequency of vacuum neutrino oscillations depends upon the magnitude of these squared-mass splitting. The larger of the two well-confirmed splittings, historically called the atmospheric splitting, is $\Delta m_{\text{atm}}^2 = 2.3 \times 10^{-3} \text{ eV}^2$ [2], while the smaller well-confirmed splitting, called the solar splitting, is $\Delta m_{\text{sol}}^2 = 7.5 \times 10^{-5} \text{ eV}^2$ [2].

On the other hand, a set of anomalous experiments provide indications of oscillations with substantially different frequency than the solar and atmospheric results. Four experiments, LSND [3], MiniBooNE [4, 5], the reactor experiments [6, 7], and the Gallium source experiments [8, 9] are consistent with a third mass splitting, $\Delta m^2 \sim 1 \text{ eV}^2$. These experiments are generally classified as “short baseline” (SBL), meaning that they are designed with a distance-to-energy ratio for the neutrino source and detector around $L/E \sim 1 \text{ m/MeV}$. LSND and MiniBooNE observed electron flavor neutrino appearance in a muon-flavored beam. The reactor and source experiments observed electron-flavor disappearance. These each represent signals in the 2σ to 4σ range, and hence are less compelling individually than the solar and atmospheric results, but taken together, the results point to a new oscillation region. To accommodate a third squared-mass splitting that is not the sum of the atmospheric and solar splittings, one must introduce a fourth neutrino mass state into the model. Since LEP Z^0 measurements are consistent with only three low mass, active

neutrinos [10], an additional fourth neutrino flavor must be inactive and is historically called sterile.

However, other SBL experiments sensitive to this higher oscillation frequency have observed null results [11–20]. In particular, muon flavor disappearance has not been observed in SBL experiments. These limits must also be accounted for in any model with extra neutrino flavors. As a result, global fits of data employing three active neutrinos and one sterile neutrino, called 3+1 models, have a limited allowed range in vacuum oscillation parameter space [21–23]. Nevertheless, 3+1 models that fit all of the data sets do remain and have prompted a suite of new SBL experiments, which are now underway [24] or are in design [25–28].

In Ref. [21], we have reported the results of global fits to the SBL data that yield allowed regions at 90% CL at three Δm^2 values at approximately 1, 1.75 and 6 eV^2 . In this paper, we expand these 3+1 fits to include a new, highly restrictive oscillation limit from the IceCube Experiment [29]. Because the IceCube analysis relies on matter effects rather than vacuum oscillations, this new data set breaks degeneracies, allowing, for the first time, to fill in all of the elements of the 3+1 mixing matrix.

INCORPORATING ICECUBE DATA INTO FITS

SBL experiments have direct sensitivity to neutrino oscillations involving electron and muon flavor neutrinos but do not have direct sensitivity to transitions involving the tau neutrino flavor. This is because the ν_τ threshold for charged current interactions of 3.4 GeV suppresses charged current interactions for these low energy SBL experiments. A full 3+1 model, however, has a 4×4 matrix that connects all three active plus single sterile flavor states to the four mass states:

$$U_{3+1} = \begin{bmatrix} U_{e1} & U_{e2} & U_{e3} & U_{e4} \\ \vdots & & \vdots & U_{\mu 4} \\ \vdots & & \vdots & U_{\tau 4} \\ U_{s1} & U_{s2} & U_{s3} & U_{s4} \end{bmatrix}. \quad (1)$$

*Corresponding author: caad@mit.edu

Due the high τ production threshold, the SBL experiments can only directly constrain the elements U_{e4} and $U_{\mu 4}$.

The observed anomalous mass splitting associated with oscillations to the fourth neutrino flavor is very large compared to the solar and atmospheric cases. Thus, for these oscillations, one can make the approximations that $\Delta m_{41}^2 \approx \Delta m_{42}^2 \approx \Delta m_{43}^2$ and $\Delta m_{21}^2 \approx \Delta m_{32}^2 \approx 0$. This leads to the SBL approximation for the vacuum oscillation probability formula for $\nu_\alpha \rightarrow \nu_\beta$

$$P_{\alpha\beta} = \delta_{\alpha\beta} - 4(\delta_{\alpha\beta} - U_{\alpha 4}U_{\beta 4}^*)U_{\alpha 4}^*U_{\beta 4}\sin^2\left(\frac{\Delta m_{41}^2 L}{4E}\right). \quad (2)$$

In this equation, L is the distance the neutrino travels and E is the energy of the neutrino. For a given choice of flavors α and β , this is equivalent to a two neutrino model with a mixing amplitude of

$$\sin^2 2\theta_{\alpha\beta} = |4(\delta_{\alpha\beta} - U_{\alpha 4}U_{\beta 4}^*)U_{\alpha 4}^*U_{\beta 4}|. \quad (3)$$

Thus, in this notation, muon-to-electron flavor appearance experiments measure $\sin^2 2\theta_{\mu e}$, and the disappearance experiments measure $\sin^2 2\theta_{ee}$ and $\sin^2 2\theta_{\mu\mu}$.

This paper makes use of the global fits to SBL data reported in Ref. [21]. The specifics of the SBL data sets given in Table 1 of this reference. The global fit favors a model with one mass state dominated by the sterile flavor. The three assumed degenerate mass states are dominated by the active flavors, as is demanded by the solar and atmospheric neutrino results. The SBL fits cannot distinguish the mass hierarchy, that is, whether the dominantly sterile flavor is the highest mass state, which is called a 3+1 hierarchy, or the lowest mass state, which is called a 1+3 hierarchy. However, cosmological bounds on neutrino mass strongly disfavor a 1+3 model [30], and so we focus on 3+1 models below.

In this paper, we expand the 3+1 fits to include data from the IceCube, which is quite different in design from the SBL experiments. It makes use of measurements of the atmospheric ν_μ flux, studied as a function of the earth zenith angle and energy in the range from 400 GeV to 20 TeV. The detector consists of 86 strings of optical modules located within the Antarctic ice near the South Pole. The energy and path-length through the Earth of these atmospheric neutrinos is equivalent to an $L/E \sim 1$ m/MeV value similar to the SBL experiments. However, the strength of the IceCube result arises from the additional MSW effect, a modification of the oscillation behavior when high energy neutrinos travel through dense matter.

The MSW signature in IceCube corresponds to a predicted large deficit in the antineutrino flux for the up-going neutrinos that cross the Earth's core [31–35]. This modification to the vacuum oscillation formalism comes from differences between neutrino charged- and neutral-current interactions with the earth. In experiments at

low energy or short baselines, this effect is negligible, and only vacuum oscillations need to be considered. However, at the high energies and long baselines available to the IceCube experiment, coherent forward scattering can significantly affects neutrino propagation. Such “matter effects” are introduced into the model through matter potentials which modify the evolution of the Schrödinger equation describing the neutrino propagation. This effect is already invoked to explain the solar neutrino deficit, where the MSW effect is due to the charge-current scattering of electron-flavor neutrinos from electrons in the sun. In a 3+1 model, an additional matter potential is introduced to account for the difference of active flavor neutrinos scattering from matter—a contribution that is missing for the sterile flavor.

The MSW effect is dependent on the neutrino mass hierarchy. In the case of a 3 + 1 hierarchy, as opposed to a 1 + 3 hierarchy, the MSW resonance will appear in the antineutrino events rather than the neutrino events. Detectable effects will lie in the range $0.01 \leq \Delta m^2 \leq 10 \text{ eV}^2$ —the region of interest for our global fits. This follows from the the resonant energy: $E_{res} = \frac{\cos 2\theta \Delta m^2}{\sqrt{2}G_F N_{nuc}}$, where θ is an effective two flavor active-to-sterile neutrino mixing angle and N_{nuc} is the target number density. The quoted sensitivity range can be understood by replacing N_{nuc} by the corresponding density of the Earth, and the energy by the energy thresholds of the data set. It should be noted that the IceCube null result leads to a more restrictive limit in the case of 1+3 compared to a 3+1 model. This comes about because about 70% of the events in IceCube are due to neutrino interactions, where a 1+3 signal would appear. This is in agreement with the conclusions of cosmology and further justifies our concentration on 3+1 models below.

Use of matter effects in the IceCube analysis breaks degeneracies in the fits, allowing, for the first time, to constrain all of the elements of the 3+1 mixing matrix. Examining Eq. 1, one sees that the matrix has elements determined by the atmospheric and solar oscillation measurements, for which we use the results of Ref. [36] as the range of allowed values. This leaves seven further elements. Four of these elements, (U_{s1}, \dots, U_{s4}) , cannot be directly constrained by experiment due to the non-interacting nature of the ‘sterile’ flavor state. However, in a 3+1 model, the mixing matrix is unitary, and so these unmeasurable elements can be determined if the remaining three matrix elements are constrained. This leaves the elements U_{e4} , $U_{\mu 4}$ and $U_{\tau 4}$ to be determined from the global fits to the combined SBL and IceCube data sets that we present below.

The SBL approximation, which has been applied in our previous fits [21], cannot be applied when including the MSW signature in IceCube. In our global analysis, the ν_{SM} values of $7.5 \times 10^{-5} \text{ eV}^2$ and $2.3 \times 10^{-3} \text{ eV}^2$ from Ref. [2] are used for Δm_{sol}^2 and Δm_{atm}^2 , respectively.

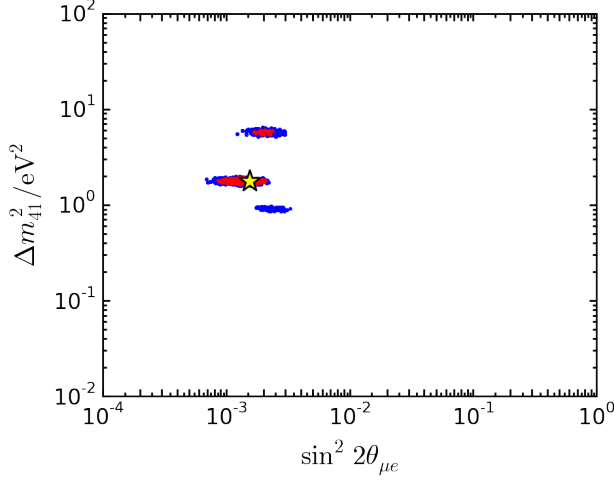


FIG. 1: Frequentist 3 + 1 global fit for SBL+IceCube: Δm_{41}^2 vs $\sin^2 2\theta_{\mu e}$. Red – 90% CL; Blue – 99% CL.

Furthermore, the introduction of IceCube data requires a parameterization of the extended lepton mixing matrix, Eq. 1. This can be presented as a product of rotations following the convention specified in Ref. [37]:

$$U_{3+1} = R_{34}R_{24}R_{14}R_{23}R_{13}R_{12}. \quad (4)$$

Each R_{ij} is a rotation matrix through angle θ_{ij} in the ij plane. In this parameterization, the fourth column of U_{3+1} is given by

$$u_4 = (\sin \theta_{14}, \cos \theta_{14} \sin \theta_{24}, \cos \theta_{14} \cos \theta_{24} \sin \theta_{34}, \cos \theta_{14} \cos \theta_{24} \cos \theta_{34})^T. \quad (5)$$

If one sets all the CP violating phases to zero, only three new angles are introduced: θ_{14} , θ_{24} , and θ_{34} . In addition, the analysis assumes $\theta_{14} = \theta_{34} = 0$. Under these assumptions, $\sin^2 2\theta_{24} = \sin^2 2\theta_{\mu\mu}$ —the vacuum disappearance amplitude. While this is a convenient way to express the ν_μ disappearance result (and is used in Ref. [29] along with other papers), these assumptions will need to be relaxed in order to include IceCube in the global fits.

The IceCube analysis and the results presented here make use of the software package called nuSQuIDS [37, 38]. This software models flavor evolution from three (*i.e.* ν SM) to six flavor basis states with customized matter potentials. The 3+1 nuSQuIDS calculation does not use the short baseline approximation; thus, it includes the two additional CP violating parameters that arise when Δm_{21}^2 and Δm_{31}^2 are nonzero and not equal. However, in the case of the IceCube analysis, these CP parameters are set to zero. For the matter potential, nuSQuIDS makes use of the Preliminary Reference Earth Model (PREM) [39] parameterization describing the radial density profile of the Earth. The neutrino propagation implementation follows Eqs. (29-30) in [40]. For the

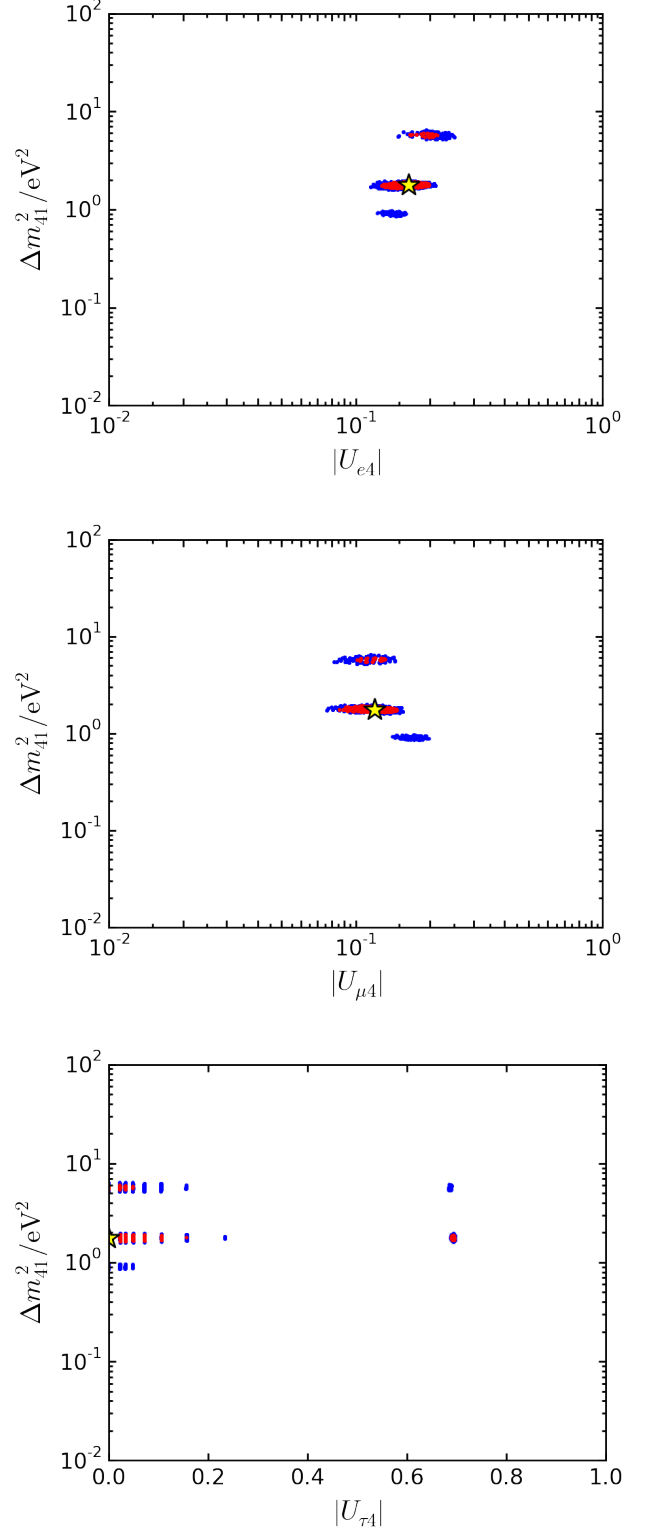


FIG. 2: Frequentist 3 + 1 global fit SBL+IceCube, shown as a function of matrix element: $|U_{e4}|$ (top), $|U_{\mu 4}|$ (middle), and $|U_{\tau 4}|$ (bottom). Red – 90% CL; blue – 99% CL.

3+1	Δm_{41}^2	$ U_{e4} $	$ U_{\mu 4} $	$ U_{\tau 4} $	N_{bins}	χ^2_{min}	χ^2_{null}	$\Delta\chi^2$ (dof)
SBL	1.75	0.163	0.117	-	315	306.81	359.15	52.34 (3)
SBL+IC	1.75	0.164	0.119	0.00	524	518.23	568.84	50.61 (4)
IC	5.62	-	0.314	-	209	207.11	209.69	2.58 (2)

TABLE I: The oscillation parameter best-fit points for $3 + 1$ for the combined SBL and IceCube data sets compared to SBL alone. Units of Δm^2 are eV^2 .

$\Delta m^2/\text{eV}^2$	$ U_{e4} $	$ U_{\mu 4} $	$ U_{\tau 4} $	θ_{34}
6	[0.17, 0.21]	[0.10, 0.13]	[0.00, 0.05]	$< 6^\circ$
2	[0.13, 0.20]	[0.09, 0.15]	[0.00, 0.70]	$< 80^\circ$

TABLE II: The 90% CL regions for matrix elements and the upper limit on θ_{34} for the two allowed regions in Δm^2 . For $\Delta m^2 = 1 \text{ eV}^2$ there are no allowed regions at 90%CL

neutrino nucleon cross sections, we use the perturbative QCD calculation from [41, 42].

No evidence for anomalous ν_μ or $\bar{\nu}_\mu$ disappearance was observed in the IceCube data set. The resulting stringent limits extends to $\sin^2 2\theta_{24} \leq 0.02$ at $\Delta m^2 \sim 0.3 \text{ eV}^2$ at 90% CL for $\theta_{34} = 0$ [29]. To incorporate this result into the fit, we must relate the mixing angles θ_{14} , θ_{24} , and θ_{34} to the short-baseline neutrino oscillation probabilities. The oscillation amplitudes in this parameterization are found by substituting the matrix elements in Eq. (5) into Eq. (2); e.g., $\sin^2 2\theta_{\mu e} = \sin^2 2\theta_{14} \sin^2 2\theta_{24}$. Since the short baseline anomalies imply $\sin^2 2\theta_{\mu e} \neq 0$, it follows that we cannot assume $\theta_{14} = 0$ in a global fit.

It has been shown [43] that the presence of the MSW resonance critically depends on the value of θ_{34} . In particular, when θ_{34} is maximal, there is no matter induced resonant enhancement. On the other hand, as noted by Ref. [32], increasing θ_{34} distorts the atmospheric ν_μ to ν_τ neutrino oscillation. The interplay between these effects makes the IceCube data sensitive to θ_{34} . We obtain the constraint on this parameter by sampling logarithmically in $\sin^2(2\theta_{34})$ from 10^{-3} to 1. The CP phases have a sub-leading contribution in comparison to the θ_{34} effect [32]; thus, they have been set to zero.

We describe the specific techniques of including the IceCube into the fits in the electronic appendix to this article. In short, the IceCube likelihood must be converted to a χ^2 that can be combined with the SBL data. The high computational cost of propagating neutrino fluxes through the Earth with nuSQUIDS prevents the analysis from being directly included into the global fitting software. Instead, the global fits were used to find a reduced set of parameters (“test points”) that could be evaluated directly. This assumes that the effect of IceCube on the global fit is a small perturbation, which is reasonable given that the IceCube-only $\Delta\chi^2$ is small compared to the SBL only global fit $\Delta\chi^2$ (see Table I).

RESULTS

Figs. 1 and 2 show the SBL+IceCube global $3 + 1$ fit result. The former shows Δm_{41}^2 vs $\sin^2 2\theta_{\mu e}$, as defined in Eq. 3. The latter presents the result as a function of mixing matrix element. The $|U_{\tau 4}|$ result is presented on a linear scale because one test point, the preferred solution, is $|U_{\tau 4}| = 0$.

The IceCube data excludes the solution at $\sim 1 \text{ eV}^2$ at 90% CL, although that solution persists at 99% CL. This has important implications for future sterile neutrino searches, in particular the Fermilab SBN program where the position of the ICARUS T600 detector was chosen to align with a large potential signal for 1 eV^2 sterile neutrinos [25].

As discussed, the SBL experiments constrain $|U_{e4}|$ and $|U_{\mu 4}|$, while the IceCube analysis has strong dependence on $|U_{\mu 4}|$ and $|U_{\tau 4}|$ through the MSW resonance. Thus, including IceCube provides insight into the less explored $|U_{\tau 4}|$ parameter. Using $|U_{\tau 4}| = \cos \theta_{14} \cos \theta_{24} \sin \theta_{34}$, we convert the results to the 90% C.L. ranges in Tab. II. At $\Delta m^2 \sim 6 \text{ eV}^2$, our limit improves the bound of $\theta_{34} < 25^\circ$ at 90% C.L. from MINOS [44] by a factor of two.

For the first time, this new result on $|U_{\tau 4}|$ allows us to have a complete picture of the extended lepton mixing matrix:

$$|U| = \begin{bmatrix} 0.79 \rightarrow 0.83 & 0.53 \rightarrow 0.57 & 0.14 \rightarrow 0.15 & 0.13 (0.17) \rightarrow 0.20 (0.21) \\ 0.25 \rightarrow 0.50 & 0.46 \rightarrow 0.66 & 0.64 \rightarrow 0.77 & 0.09 (0.10) \rightarrow 0.15 (0.13) \\ 0.26 \rightarrow 0.54 & 0.48 \rightarrow 0.69 & 0.56 \rightarrow 0.75 & 0.0 (0.0) \rightarrow 0.7 (0.05) \\ \dots & \dots & \dots & \dots \end{bmatrix}. \quad (6)$$

Above, “...” represents parameters constrained by the overall unitarity of the 4×4 matrix. The ranges in the matrix correspond are a 90% confidence interval. The entries in the last column correspond to this work and are given for $\Delta m^2 \sim 2 \text{ eV}^2$ ($\Delta m^2 \sim 6 \text{ eV}^2$). The intervals shown in each entry for the standard 3×3 submatrix were obtained from Ref. [45], and are independent of our fit. As a check of consistency, our values in the fourth column can be compared with the upper bounds from the 3×3 non-unitarity analysis in Ref. [45], which gave $|U_{e4}| < 0.27$, $|U_{\mu 4}| < 0.73$, and $|U_{\tau 4}| < 0.623$ at 90%CL. Our results in Eq. 6 are fully compatible with these upper limits, which are based on standard 3-neutrino oscillation measurements exclusive of any sterile neutrino

search data.

CONCLUSION

We have presented three new results. First, we have presented a combined fit of SBL and IceCube data resulting in a best fit of $\Delta m_{41}^2 = 1.75 \text{ eV}^2$ with $\Delta\chi_{\text{null-min}}^2$ of 50.61 for 4 dof. We have shown that this fit is sensitive to $|U_{\tau 4}|$, providing the best constraint to date on $\theta_{34} < 6^\circ$ at 90% C.L. for $\Delta m_{41}^2 > 2 \text{ eV}^2$. Lastly, we have used this, along with constraints from fits to atmospheric and solar data sets, to fill in all components of the 3+1 mixing matrix for the first time.

Acknowledgements

GC, CA and JC are supported by NSF grants 1505858 and 1505855, and MS is supported by NSF grant 1404209. We thank Christina Ignarra, Benjamin Jones, William Louis, and Jordi Salvado for useful discussion. We thank Maxim Goncharov for computing support.

- [1] K. A. Olive et al. (Particle Data Group), *Chin. Phys.* **C38**, 090001 (2014).
- [2] M. Gonzalez-Garcia, M. Maltoni, and T. Schwetz, *Journal of High Energy Physics* **2014**, 52 (2014), URL <http://dx.doi.org/10.1007/JHEP11%282014%29052>.
- [3] A. Aguilar-Arevalo et al. (LSND Collaboration), *Phys. Rev. D* **64**, 112007 (2001).
- [4] A. A. Aguilar-Arevalo et al. (MiniBooNE), *Phys. Rev. Lett.* **110**, 161801 (2013), 1207.4809.
- [5] A. A. Aguilar-Arevalo et al. (MiniBooNE), *Phys. Rev. Lett.* **102**, 101802 (2009), 0812.2243.
- [6] Y. Declais, J. Favier, A. Metref, H. Pessard, B. Achkar, et al., *Nucl. Phys. B* **434**, 503 (1995).
- [7] G. Mention, M. Fechner, T. Lasserre, T. A. Mueller, D. Lhuillier, M. Cribier, and A. Letourneau, *Phys. Rev. D* **83**, 073006 (2011), 1101.2755.
- [8] J. Abdurashitov et al. (SAGE Collaboration), *Phys. Rev. C* **80**, 015807 (2009).
- [9] F. Kaether, W. Hampel, G. Heusser, J. Kiko, and T. Kirsten, *Phys. Lett. B* **685**, 47 (2010).
- [10] ALEPH Collaboration, DELPHI Collaboration, L3 Collaboration, OPAL Collaboration, SLD Collaboration, LEP Electroweak Working Group, SLD Electroweak and Heavy Flavour Groups, *Phys. Rept.* **427**, 257 (2006).
- [11] B. Armbruster et al. (KARMEN Collaboration), *Phys. Rev. D* **65**, 112001 (2002).
- [12] J. Conrad and M. Shaevitz, *Phys. Rev. D* **85**, 013017 (2012).
- [13] P. Adamson et al. (MiniBooNE and MINOS Collaborations), *Phys. Rev. Lett.* **102**, 211801 (2009).
- [14] A. A. Aguilar-Arevalo et al. (MiniBooNE Collaboration), *Phys. Rev. Lett.* **103**, 061802 (2009).
- [15] G. Cheng et al. (SciBooNE Collaboration), *Phys. Rev. D* **84**, 012009 (2011).
- [16] P. Astier et al. (NOMAD Collaboration), *Phys. Lett. B* **570**, 19 (2003).
- [17] I. Stockdale, A. Bodek, F. Borchering, N. Giokaris, K. Lang, et al., *Z. Phys. C* **27**, 53 (1985).
- [18] F. Dydak, G. Feldman, C. Guyot, J. Merlo, H. Meyer, et al., *Phys. Lett. B* **134**, 281 (1984).
- [19] D.G. Michael *et al.* (MINOS Collaboration), *Phys. Rev. Lett.* **97**, 191801 (2006).
- [20] P. Adamson *et al.* (MINOS Collaboration), *Phys. Rev. Lett.* **101**, 131802 (2008).
- [21] G. H. Collin, C. A. Argelles, J. M. Conrad, and M. H. Shaevitz, *Nucl. Phys.* **B908**, 354 (2016), 1602.00671.
- [22] J. Kopp, P. A. N. Machado, M. Maltoni, and T. Schwetz, *Journal of High Energy Physics* **2013** (2013), ISSN 1029-8479, arXiv: 1303.3011, URL <http://arxiv.org/abs/1303.3011>.
- [23] C. Giunti, M. Laveder, Y. F. Li, and H. W. Long, *Physical Review D* **88** (2013), ISSN 1550-7998, 1550-2368, arXiv: 1308.5288, URL <http://arxiv.org/abs/1308.5288>.
- [24] H. Chen *et al.* (MicroBooNE Collaboration) (2007), “Proposal for a New Experiment Using the Booster and NuMI Neutrino Beamlines: MicroBooNE”, URL http://www-microboone.fnal.gov/public/MicroBooNE_10152007.pdf.
- [25] M. Antonello et al. (LAr1-ND, ICARUS-WA104, MicroBooNE) (2015), 1503.01520.

- [26] A. Adelmann, J. Alonso, W. A. Barletta, J. M. Conrad, M. H. Shaevitz, J. Spitz, M. Touns, and L. A. Winslow, *Adv. High Energy Phys.* **2014**, 347097 (2014), 1307.6465.
- [27] T. J. Langford (PROSPECT), *Nucl. Part. Phys. Proc.* **265-266**, 123 (2015), 1501.00194.
- [28] D. Bravo-Berguo et al. (SOX), *Nucl. Part. Phys. Proc.* **273-275**, 1760 (2016).
- [29] M. G. Aartsen et al. (IceCube) (2016), 1605.01990.
- [30] P. A. R. Ade et al. (Planck) (2015), 1502.01589.
- [31] S. Razzaque and A. Yu. Smirnov, *Phys. Rev.* **D85**, 093010 (2012), 1203.5406.
- [32] A. Esmaili and A. Yu. Smirnov, *JHEP* **12**, 014 (2013), 1307.6824.
- [33] V. Barger, Y. Gao, and D. Marfatia, *Phys. Rev.* **D85**, 011302 (2012), 1109.5748.
- [34] A. Esmaili, F. Halzen, and O. L. G. Peres, *JCAP* **1211**, 041 (2012), 1206.6903.
- [35] A. Esmaili, F. Halzen, and O. L. G. Peres, *JCAP* **1307**, 048 (2013), 1303.3294.
- [36] S. Parke and M. Ross-Lonergan (2015), 1508.05095.
- [37] C. A. Argüelles Delgado, J. Salvado, and C. N. Weaver (2014), 1412.3832.
- [38] C. A. Argüelles Delgado, J. Salvado, and C. N. Weaver, *ν -SQuIDS*, <https://github.com/arguelles/nuSQuIDS>.
- [39] A. M. Dziewonski and D. L. Anderson, *Physics of the Earth and Planetary Interiors* **25**, 297 (1981).
- [40] M. C. Gonzalez-Garcia, F. Halzen, and M. Maltoni, *Phys. Rev.* **D71**, 093010 (2005), hep-ph/0502223.
- [41] C. A. Argüelles, F. Halzen, L. Wille, M. Kroll, and M. H. Reno, *Phys. Rev.* **D92**, 074040 (2015), 1504.06639.
- [42] A. Cooper-Sarkar, P. Mertsch, and S. Sarkar, *JHEP* **08** (2011), 1106.3723, URL <http://arxiv.org/abs/1106.3723>.
- [43] M. Lindner, W. Rodejohann, and X.-J. Xu (2015), 1510.00666.
- [44] P. Adamson et al. (MINOS), *Phys. Rev. Lett.* **107**, 011802 (2011), 1104.3922.
- [45] S. Parke and M. Ross-Lonergan (2016), private communication.
- [46] M. Honda, T. Kajita, K. Kasahara, and S. Midorikawa, *Phys. Rev. D* **70**, 043008 (2004).
- [47] <http://icecube.wisc.edu/science/data/IC86-sterile-neutrino> (2016).
- [48] B. J. P. Jones, Ph.D. thesis, MIT (2015), URL <http://lss.fnal.gov/archive/thesis/2000/fermilab-thesis-2015-17.pdf>.
- [49] C. A. Argüelles Delgado, Ph.D. thesis, University of Wisconsin - Madison (2015), URL <http://search.proquest.com/docview/1720322773>.

Appendix: Incorporating the IceCube Data Into the Fits

The fits proceed by first obtaining the prediction for IceCube for a given 3+1 model. To obtain this, we use the Honda-Gaisser [46] prediction for the unoscillated flux. The nuSQuIDS package [38] is used to propagate the neutrino flux across the Earth. The software solves the neutrino evolution “master equation” that accounts for absorption, regeneration and oscillations (Eqs. (29-30) in Ref. [40]). A propagated flux hypothesis is used to produce a weight for each neutrino energy, zenith angle and flavor at the detector. This can then be used to re-weight the IceCube simulated events available in Ref. [47].

The IceCube likelihood is given by [29, 48, 49]:

$$\ln \mathcal{L}(\vec{\theta}) = \min_{\eta} \left(\sum_{i=1}^{N_{bins}} \left[x_i \ln \mu_i(\vec{\theta}; \eta) - \mu_i(\vec{\theta}; \eta) - \ln x_i! \right] + \frac{1}{2} \sum_{\eta} \frac{(\eta - \bar{\eta})^2}{\sigma_{\eta}^2} \right), \quad (7)$$

where x_i are the number of events in the i th bin, μ_i is the MC expectation in the same bin, given nuisance parameters (η) and oscillation parameters ($\vec{\theta}$).

We include the nuisance parameters specified in [29, 47–49]. We maximize the likelihood as a function of flux variants at each parameter point. We note this is an important step in reproducing the IceCube limit.

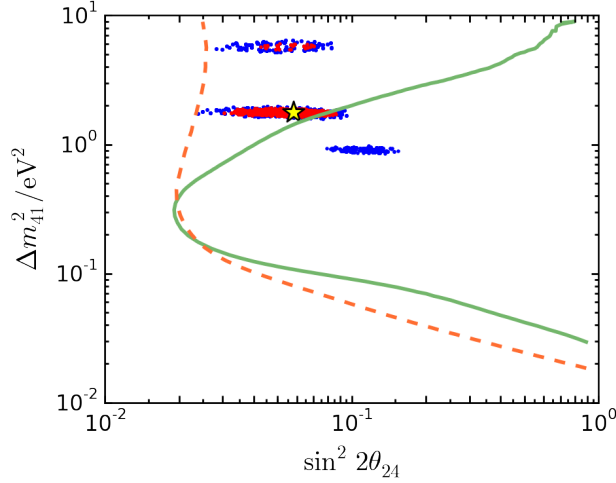
In Supplementary Figure 1, we show the IceCube 90% CL limit obtained by this analysis. As expected, the result for $\theta_{34} = 0^\circ$, shown by the solid line, is in agreement with that presented in Refs. [29, 48, 49] for the “rate+shape” analysis. This limit is modified at high δm^2 if θ_{34} is nonzero, as discussed in Ref. [43]. We illustrate the effect with the 90% CL limit for IceCube assuming $\theta_{34} = 15^\circ$, shown by the dashed line. Also overlaid on this plot is the global fit result, including the IceCube result, expressed as a function of Δm_{41}^2 vs $\sin^2 2\theta_{24}$.

In order to combine the IceCube result with the other experiments in Table 1 of Ref. [21], the IceCube likelihood must be converted to a χ^2 that can be combined with that of the global fit. In order to do this, it is convenient to use:

$$\ln \mathcal{LR}(\vec{\theta}) = \ln \left(\frac{\mathcal{L}(\sin^2 2\theta_{24}, \Delta m_{41}^2)}{\mathcal{SP}(\{x_i\})} \right), \quad (8)$$

where $\mathcal{SP}(\{x_i\}) = \prod_i \mathbb{P}_{poisson}(x_i|x_i)$ is the saturated Poisson. In the fitting code, we implement Eq. 7, and in Tab. I we use Eq. 8, following the same procedure as for LSND and Karmen. (The definitions in Eq. 7 and Eq. 8 give the same $\Delta \ln \mathcal{L}$ used for fitting and parameter estimation.)

The high computational cost of propagating neutrino fluxes through the Earth with nuSQuIDS prevents the



SUPPL. FIG. 1: The solid (dashed) line represents the 90% C.L. IceCube limit when calculated with $\theta_{34} = 0^\circ$ ($\theta_{34} = 15^\circ$). The result of the SBL+IC global fit is overlaid, Red – 90% CL; blue–99% CL.

analysis from being directly included into the global fitting software. Instead, the global fits were used to find a reduced set of parameters (called “parameter-set points” below) that could be evaluated directly. The 60,000 parameter-set points for the SBL global fits from Ref. [21], *i.e.* without IceCube data included, with the lowest χ^2 were used. From these every 40th point was selected. This gave a fine sampling of the global fit near the minima. Of the remaining $\approx 140,000$ parameter-set points that are far from the minima, every 60th was selected. Combining the fine sample and the coarse sample yields 4,000 points. These 4,000 selected parameter-set points only explored changes in the values for θ_{14} and θ_{24} . In order to incorporate the IceCube data and effects of θ_{34} , ten values of the θ_{34} angle were chosen for each parameter point, resulting in a total of 40,000 parameter-set points. These points were fed into the IceCube analysis likelihood and the resulting χ^2 value, defined by Eq. 8, was combined with the respective frequentist global fit χ^2 .

This assumes that the effect of IceCube on the global fit is a small perturbation. This is reasonable given that the IceCube-only $\Delta\chi^2$ is small compared to the SBL only global fit $\Delta\chi^2$, as shown in Table I.